

This is an electronic reprint of the original article. This reprint may differ from the original in pagination and typographic detail.

---

## Numerical Study of Gas Flow and Temperature Patterns in the Blast Furnace Throat

Mondal, Debanga; Liu, Weiqiang; Bartusch, Hauke; Kaymak, Yalcin; Paananen, Timo; Mattila, Olli; Saxén, Henrik

*Published in:*

Metallurgical and Materials Transactions B: Process Metallurgy and Materials Processing Science

*DOI:*

[10.1007/s11663-022-02649-5](https://doi.org/10.1007/s11663-022-02649-5)

Published: 01/12/2022

*Document Version*

Final published version

*Document License*

CC BY

[Link to publication](#)

*Please cite the original version:*

Mondal, D., Liu, W., Bartusch, H., Kaymak, Y., Paananen, T., Mattila, O., & Saxén, H. (2022). Numerical Study of Gas Flow and Temperature Patterns in the Blast Furnace Throat. *Metallurgical and Materials Transactions B: Process Metallurgy and Materials Processing Science*, 53(6), 3882-3895. <https://doi.org/10.1007/s11663-022-02649-5>

### General rights

Copyright and moral rights for the publications made accessible in the public portal are retained by the authors and/or other copyright owners and it is a condition of accessing publications that users recognise and abide by the legal requirements associated with these rights.

### Take down policy

If you believe that this document breaches copyright please contact us providing details, and we will remove access to the work immediately and investigate your claim.

# Numerical Study of Gas Flow and Temperature Patterns in the Blast Furnace Throat



DEBANGA NANDAN MONDAL, WEIQIANG LIU, HAUKE BARTUSCH,  
YALCIN KAYMAK, TIMO PAANANEN, OLLI MATTILA, and HENRIK SAXÉN

The gas distribution in the shaft is of key importance for the performance of the blast furnace process, since it affects the way in which the burden is heated and reduced, and also the pressure drop in the shaft and cohesive zone. Traditionally, the gas distribution is followed by gas temperature measurements at several points over the radius or diagonal by the above-burden probes, but novel acoustic techniques can estimate the gas temperature over the full cross section of the throat. A fundamental problem is that the gas is redistributed in the upper bed and above it, so the measured profile may no longer reflect the conditions in the shaft. This paper studies the gas redistribution by a CFD model of the throat region, neglecting heat transfer to the bed and walls. It is demonstrated that strong redistribution and downward-swirling flows may occur, which affect the measurements. The arising conditions under different assumptions of the bed state are studied, and the dynamics of the changes are also briefly analyzed. A comparison of the findings of the computational model with acoustic measurements of the gas temperatures in the throat of two industrial blast furnaces reveals a good resemblance. The results of the study sheds light on the complex flow conditions of the gas in the blast furnace throat region and can be used to interpret information from measuring devices and to study how their positioning affects the measurements.

<https://doi.org/10.1007/s11663-022-02649-5>

© The Author(s) 2022

## I. INTRODUCTION

THE blast furnace is the predominant process for the production of molten iron for steelmaking, and the process has been studied extensively over the years using mathematical modeling.<sup>[1,2]</sup> The radial distribution of the gas in the blast furnace is an important variable for the performance of the process as it affects heat and mass transfer in the furnace shaft and, through these, the efficiency of the indirect reduction reactions of iron oxides.<sup>[3–6]</sup> The gas distribution can be controlled indirectly by manipulating the way in which the burden is charged into the furnace,<sup>[7–10]</sup> but it may also vary spontaneously due to uncontrolled changes in the state of the shaft and cohesive zone. To gain a better

understanding of the gas distribution, horizontal or inclined probes have been applied above or below the burden surface.<sup>[3,11,12]</sup> These typically measure the temperatures and sometimes take gas samples to determine the gas composition at a number of discrete points along one radius. The in-burden probes also sample gas, while the above-burden probes usually only measure temperatures. The above-burden probes are quite often configured in a diagonal or double-diagonal fashion, giving information about possible peripheral differences. The in-burden probes, which typically only measure along one radius, are known to yield more accurate information, but they can only be applied intermittently and have to be withdrawn after the temperature measuring and gas sampling have been undertaken. Therefore, this information is available only once per shift or day. Even though the above-burden probes provide practically continuous information, a problem associated with such sampling is a possible redistribution of the gas before the probe.<sup>[3,13]</sup> This means that the results do not necessarily reflect the conditions of the gas in the shaft. The problem can be somewhat relaxed by placing the probes as close to the burden surface as possible, but this is challenging as a possible upward motion of the bed may at disturbances may bend or destroy the probes so a sufficient safety distance to the stockline must be maintained. A more serious problem

---

DEBANGA NANDAN MONDAL, WEIQIANG LIU, and HENRIK SAXÉN are with the Process and Systems Engineering, Åbo Akademi University, 20500 Åbo, Finland. Contact e-mail: [weiqiang.liu@abo.fi](mailto:weiqiang.liu@abo.fi) HAUKE BARTUSCH and YALCIN KAYMAK are with the VDEh Betriebsforschungsinstitut, Sohnstrasse 63, D 45894 Rastatt, Germany. TIMO PAANANEN and OLLI MATTILA are with the SSAB Europe Raahe, Rautaruukintie 155, 92100 Raahe, Finland.

Manuscript submitted May 11, 2022; accepted September 4, 2022.

Article published online October 5, 2022.

is that the gas may not only redistribute, but even exhibit a downward flow locally due to the complex gas flow patterns in the throat region.<sup>[13,14]</sup> Also novel acoustic-based methods for estimating the gas temperature distribution over the cross section (see, *e.g.*, References 15 through 18) have in studies by the authors of the present paper indicated the presence of such downward flow in the regions between the gas uptakes.

In order to gain a better understanding of the fate of the blast furnace gas as it passes through the uppermost burden layers and enters the throat region above the stockline, a CFD study of the system under different states was undertaken. The region considered extends from the upper part of the burden bed into the four gas uptakes, and studies the gas flow and temperature. The findings provide evidence of complex flow patterns, where gas from different regions is mixed, giving insight that can be used when the location or feasibility of measurement devices is studied.

Section II of the paper presents the simulation domain and the assumptions made in the modeling. The results are presented in Section III, while Section IV briefly discusses the dynamics of the system. Section V presents some results of temperature patterns measured by acoustic techniques in two larger blast furnace, and qualitatively compares them with findings of the numerical analysis. Section VI finally presents conclusions of the work and proposes potential topics to be studied in the future.

## II. MATHEMATICAL MODEL

The system studied in this work consists of the upper part of the burden bed in the throat region of the blast furnace, further including about 4 m of the gas uptakes. Even though the conditions studied are symmetric, a three-dimensional representation is used here. The geometry of the furnace was taken from an industrial

blast furnace (called BF A) that acted as a reference for the study. While the upper part of the throat and gas uptakes only hold gas, the lower part of the throat is occupied by burden, described as a porous medium, and the ascending gas. Figure 1 shows the simulated domain and its two distinct parts, as well as the dimensions.

To mimic the conditions in the blast furnace, a gas with a given temperature distribution along the radius (illustrated in Figure 2) was introduced at the lower end of the domain. The distribution was selected based on common temperature patterns measured by an above-burden probe in the reference blast furnace. The gage pressure at the inlet was set to 132 kPa and at the outlet at 130 kPa; this pressure difference was found to result in a top gas volume flow rate ( $35 \text{ m}^3/\text{s}$ ) resembling the calculated one in the reference blast furnace.

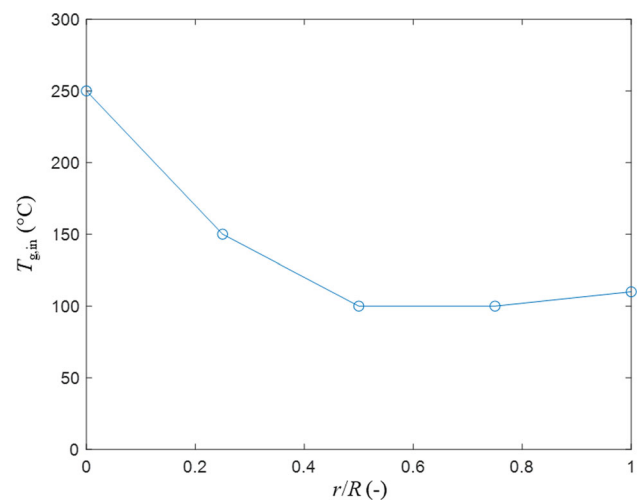


Fig. 2—Radial distribution of inlet gas temperature.

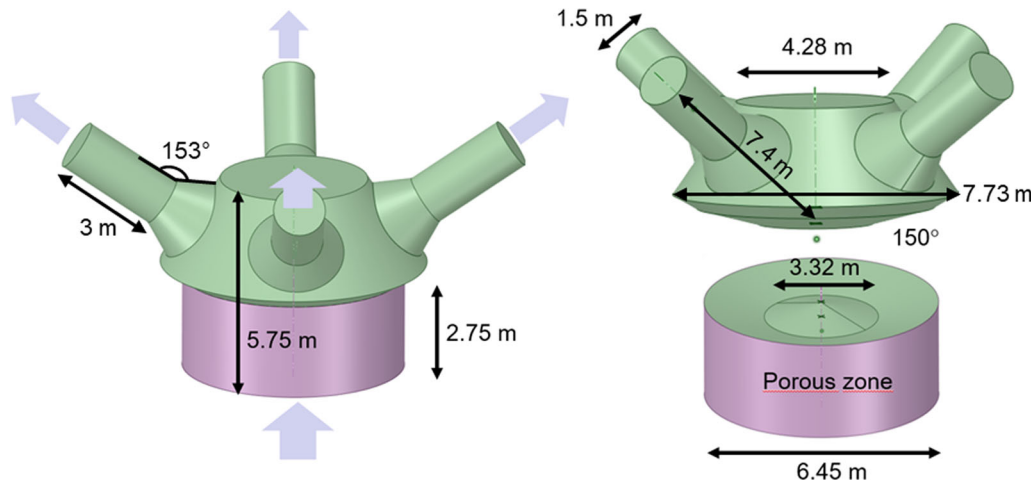


Fig. 1—Simulated domain and dimensions.

It should be noted that the present study is focused on the behavior of the gas flow only, and its effect on the gas temperature in the domain. Therefore, the system is considered adiabatic and no heat transfer between the gas and the burden or between the gas and the walls is considered. Because of this, the burden bed is considered static, even though it in practice descends. This assumption simplifies the treatment significantly. To consider the distributing effect of the burden bed on the gas flow, the bed was discretized into concentric regions of different porosities, as outlined in Figure 3 and particle sizes as reported in Table I. In the figure, the lower beige part is the base bed, upon which an optional heap (“center coke” or “center pellet”) can be added. This porosity distribution of the bed gives rise to a higher gas velocity in the furnace center, which is common in blast furnaces due to charging of more coke in this region, while the region dominated by pellets at the wall has a lower permeability, and hence a weaker gas flow.<sup>[19]</sup> The parameters of the bed and the heap are given in Table I.

The system was studied based on the ANSYS Fluent 2020 platform. The basic governing equations of the model are

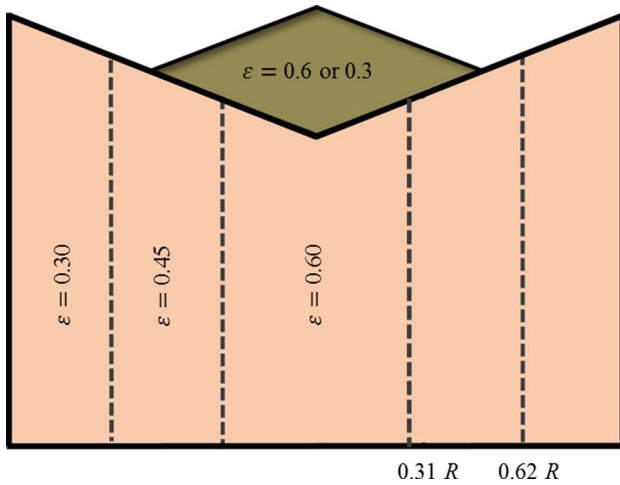


Fig. 3—Description of the burden bed by division into regions of different permeabilities.

$$\frac{\partial}{\partial t}(\varepsilon \rho_g) + \nabla \cdot (\varepsilon \rho_g \mathbf{u}) = 0, \quad [1]$$

$$\begin{aligned} \frac{\partial}{\partial t}(\varepsilon \rho_g \mathbf{u}) + \nabla \cdot (\varepsilon \rho_g \mathbf{u} \mathbf{u}) = & \nabla \cdot [\varepsilon(\eta + \eta_t)(\nabla \mathbf{u} + \nabla \mathbf{u}^T)] \\ & + \varepsilon(\rho_g \mathbf{g} - \nabla p - \mathbf{R}), \end{aligned} \quad [2]$$

$$\begin{aligned} [\rho_s c_{p,s}(1 - \varepsilon) + \rho_g c_{p,g} \varepsilon] \left( \frac{\partial T}{\partial t} + \mathbf{u} \cdot \nabla T \right) \\ = \nabla \cdot [(k_g + k_{g,t})\varepsilon + k_s(1 - \varepsilon)] \nabla T, \end{aligned} \quad [3]$$

where  $t$ ,  $\varepsilon$ ,  $\mathbf{u}$ ,  $\mathbf{g}$ ,  $\eta$ ,  $p$ , and  $T$  are time, porosity, velocity vector, gravitational acceleration, viscosity, pressure, and temperature, while  $\rho_g$ ,  $c_{p,g}$ ,  $k_g$ ,  $\rho_s$ ,  $c_{p,s}$ ,  $k_s$  are the density, heat capacity, and thermal conductivity for the gas and solid material. The last term ( $\mathbf{R}$ ) of Eq. [2] is the flow resistance in the burden and is described by the well-known Ergun equation

$$\mathbf{R} = \frac{\varepsilon}{A} \eta \mathbf{u} + \frac{\varepsilon^2 B}{2} \rho_g \mathbf{u} |\mathbf{u}|, \quad [4]$$

where  $A$  is the permeability of the burden and  $B$  is the inertial term accounting for the kinetic energy of turbulent eddies. The two parameters are expressed by

$$A = \frac{d_p^2}{150} \frac{\varepsilon^3}{(1 - \varepsilon)^2}; B = \frac{3.5}{d_p} \frac{1 - \varepsilon}{\varepsilon^3} \quad [5]$$

where  $d_p$  is effective size of burden particle.

The ‘realizable k-epsilon’ viscous model was used to describe the turbulent viscosity ( $\eta_t$ ) and turbulent gas thermal conductivity ( $k_{g,t}$ ).

For the sake of simplicity, the gas was taken to be air. As for the boundary conditions of the model, pressure boundary conditions were applied at the lower and upper ends of the system. Inlet temperature was provided by using user-defined boundary condition. A grid of about 149,000 cells was applied, which was found sufficient to guarantee grid-independent solutions. The system was simulated until a stable steady state was achieved (except in the dynamic cases presented in [Dynamic Analysis](#)).

Table I. Conditions for the Different Bed Parts Studied (cf. Fig. 3)

Part	Material	Particle Size	Voidage
Base Bed	coke + pellet	30 mm	0.30/0.45/0.60
Center Heap	coke or pellet	50 mm or 10 mm	0.60 or 0.30

### III. STATIC ANALYSIS

This section studied the system in steady-state, focusing on the resulting gas temperature and flow fields. Section III-A illustrates the results for the vertical and horizontal cross sections indicated in Figure 4, while Section III-B provides some three-dimensional views to gain a better understanding of the complex gas flow in the blast furnace throat. The two vertical planes go through the center of the gas uptakes (Figure 4(a)) or halfway between them (Figure 4(b)), while the horizontal planes (Figure 4(c)) are at the vertical levels  $-1.00$  m,  $-0.50$  m,  $0.00$  m, and  $+0.25$  m, where the highest level of the burden surface at the throat wall is  $0.00$  m.

#### A. Two-Dimensional Views

The system was first simulated with the base bed, labeled Case 1 (cf. first row of Table II). The arising steady-state gas temperature and velocity pathlines are shown in Figure 5. The hot central gas zone (Figure 5(a)) is seen to converge somewhat above the burden surface, flowing toward the ceiling to divert toward the two gas uptakes. The local acceleration of the gas in this region is clearly seen in Figure 5(b), as well as the higher gas flow velocity in the uptakes, because their joint cross-section area is only about a fifth of the throat cross-section area.

While these findings are quite intuitive, the conditions at a vertical plane halfway between the gas uptakes (*i.e.*,  $45^\circ$  off from that studied in Figure 5) are fundamentally different. Even though the conditions of the central gas flow are naturally similar (as it basically represents the same as in the previous figure), the conditions at the conical top wall are very different. After hitting the ceiling, the gas cannot straightforwardly be diverted to the uptakes, but instead has to flow downwards along the wall, creating a swirl (see Section III-B) toward the closest gas uptake, *i.e.*, perpendicular to the represented plane. As seen in Figure 6(b), this gives rise to a higher temperatures (about  $413$  K ( $140^\circ\text{C}$ ), represented by turquoise color) along the wall, forming a rotating flow. This phenomenon was discussed by Timmer *et al.*<sup>[14]</sup> in an early study of the problem, which pointed out implications of it for gas temperatures measurements by the above-burden probes. The downward and swirling flow is particularly detrimental for new 2-dimensional noncontact gas temperature measurements by acoustic techniques, as discussed in more detail in Section III-B, since it gives rise to spurious high-temperature zones not reflecting the radial temperature distribution of the gas temperature that enters from the shaft.

The left column of Figure 7 shows the gas temperatures along horizontal planes on five vertical levels in the throat region, corresponding to the entrance of the bed (*i.e.*, lower boundary conditions) at the bottom row and the four levels are indicated in Figure 4(c). The fourth row represents the temperatures at  $z = -1.00$  m, *i.e.*, a cross section that falls entirely within the burden bed,  $z = -0.50$  m a level that partly falls in the bed (at the wall) and partly above it (in the center), while the uppermost two level ( $z = 0.00$  m and  $z = 0.25$  m) are

above the bed, where the former barely touches the bed surface at the wall. These figures show that the gas temperature distribution remains relatively unchanged until it reaches the top level, but changes strongly above the bed due to the downward flow of the hot gas originating in the furnace center for the regions between the gas uptakes. (The radial positions of the uptakes have been indicated by dashed red circles in the topmost figure.) Thus, any device that directly or indirectly measures the gas temperature above the burden surface is prone to misinterpret the conditions in the shaft: while the temperatures in the furnace center are sensed relatively accurately, the temperatures at the wall show considerable differences and particularly so between the gas uptakes.

Next, the effect of coke (Case 2) or pellets (Case 3) charged in the center (cf. Figure 3) is studied. The former alternative is quite commonly encountered in charging program of industrial blast furnaces, where it is known to promote central flow of the gas, which is associated with a low pressure drop and stable burden descent. The latter case, in turn, is not common but is here merely included to show the impact on the gas flow distribution in the throat.

For the plane intersecting two gas uptakes (Figure 8), the center-coke dump is seen to divert the gas toward the uptakes, which clearly lowers the temperatures higher up in the central part (Figure 8(a)). Above the coke heap, the gas creates a back swirl (Figure 8(b)). The situation along a plane halfway between the uptakes (Figure 9) is also changed: as the strong central flow to the ceiling is fully suppressed, the downward swirl is replaced by a backward swirl in the wake above the coke heap. This serves to better preserve the gas temperature distribution in the burden also above the bed surface, as seen in the second column of Figure 7. However, the coke heap distributes the gas in the center, which somewhat increases the extent of the high-temperature region, and simultaneously lowers its temperature.

The results of a similar study of a center-pellet dump (Case 3) are presented in Figures 10 and 11 and in the rightmost column of Figure 7. As expected, the denser bed of smaller particles and lower voidage (cf. Table I) exerts a stronger “splitting” effect on the center gas flow, which diverges toward the uptakes. This widens the wake zone above the center heap, and yields a larger circular region of rather constant temperature of about  $413$  K ( $140^\circ\text{C}$ ) above the bed, as indicated by the green region in the top right panel of Figure 7. The backward swirl above the pellet heap is particularly strong in the plane between the uptakes (Figure 11), from where it rotates in the direction perpendicular to the plane toward a close gas uptake, as illustrated in Section III-B.

The modifying effects of the center heaps on the gas velocity distribution can be studied in more detail in Figure 12, which depicts the gas velocities by colored arrows for the vertical plane through the gas uptakes for Cases 1–3. For the base bed (Case 1, Figure 12a), the strong convergence and acceleration of the gas above the bed in the center is seen. From an entrance velocity ranging between  $0.5$  m/s at the wall) and  $3$  m/s (at the



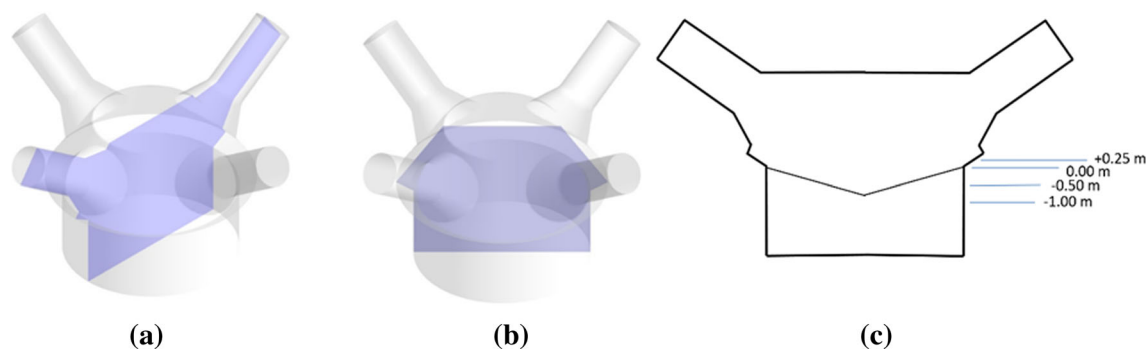


Fig. 4—(a, b) Vertical and (c) horizontal planes along which the simulated gas temperatures and flow are studied.

**Table II. Conditions for the Different Bed Parts Studied (cf. Fig. 3)**

Case #	Base Bed	Center Heap
1	coke + pellet	—
2	coke + pellet	coke
3	coke + pellet	pellet

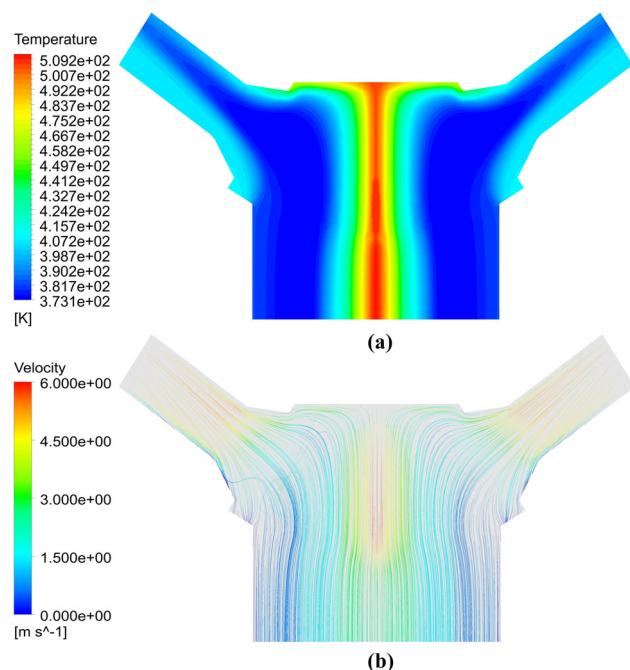


Fig. 5—Base bed (Case 1): (a) Gas temperatures and (b) velocity pathlines for a vertical plane intersecting two gas uptakes (cf. Fig. 4a) (Color figure online).

center), as seen in Figure 13, the gas accelerates to almost 6 m/s to retard as the ceiling is approached, where the gas is diverted outwards radially. The center coke on the base bed (Case 2, Figure 12(b)) represents an additional flow resistance, which deflects the stronger central flow within the bed toward the heap surfaces, which creates a strong gas flow almost directly toward the gas uptakes.

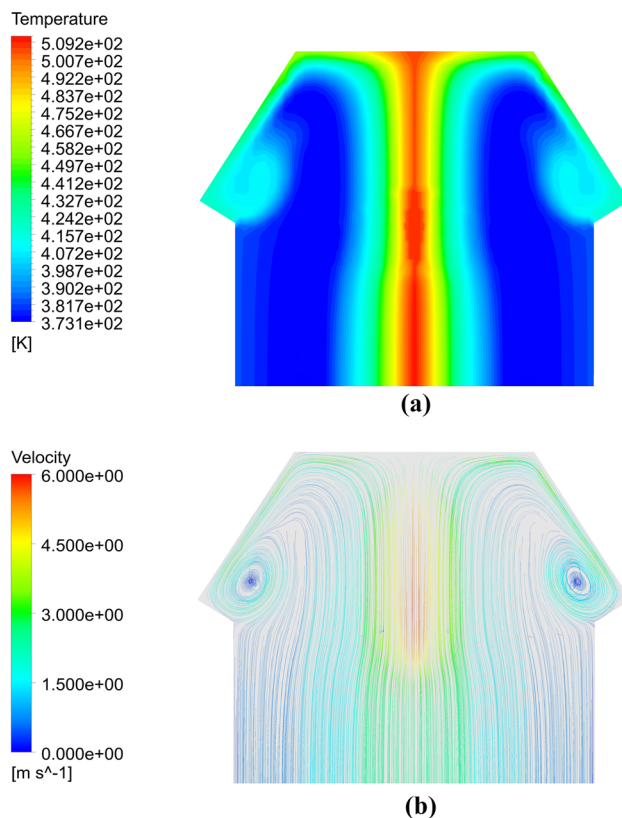


Fig. 6—Base bed (Case 1): (a) Gas temperatures and (b) velocity pathlines for a vertical plane halfway between two gas uptakes (cf. Fig. 4b) (Color figure online).

This creates a wake above the heap, where the gas swirls downwards in the opposite direction to the main flow to the uptakes. The deflected gas flow from the center is seen to go out practically perpendicular to the coke-heap surface. The charging of a center-pellet dump (Case 3, Figure 12(c)), in turn, efficiently blocks the center. The gas flow from the center now practically avoids the heap and flows out around the radial position of the heap edge. This increases the peripheral flow, with the strongest velocities encountered at the outer edge of the heap, giving rise to a large wake region in the center

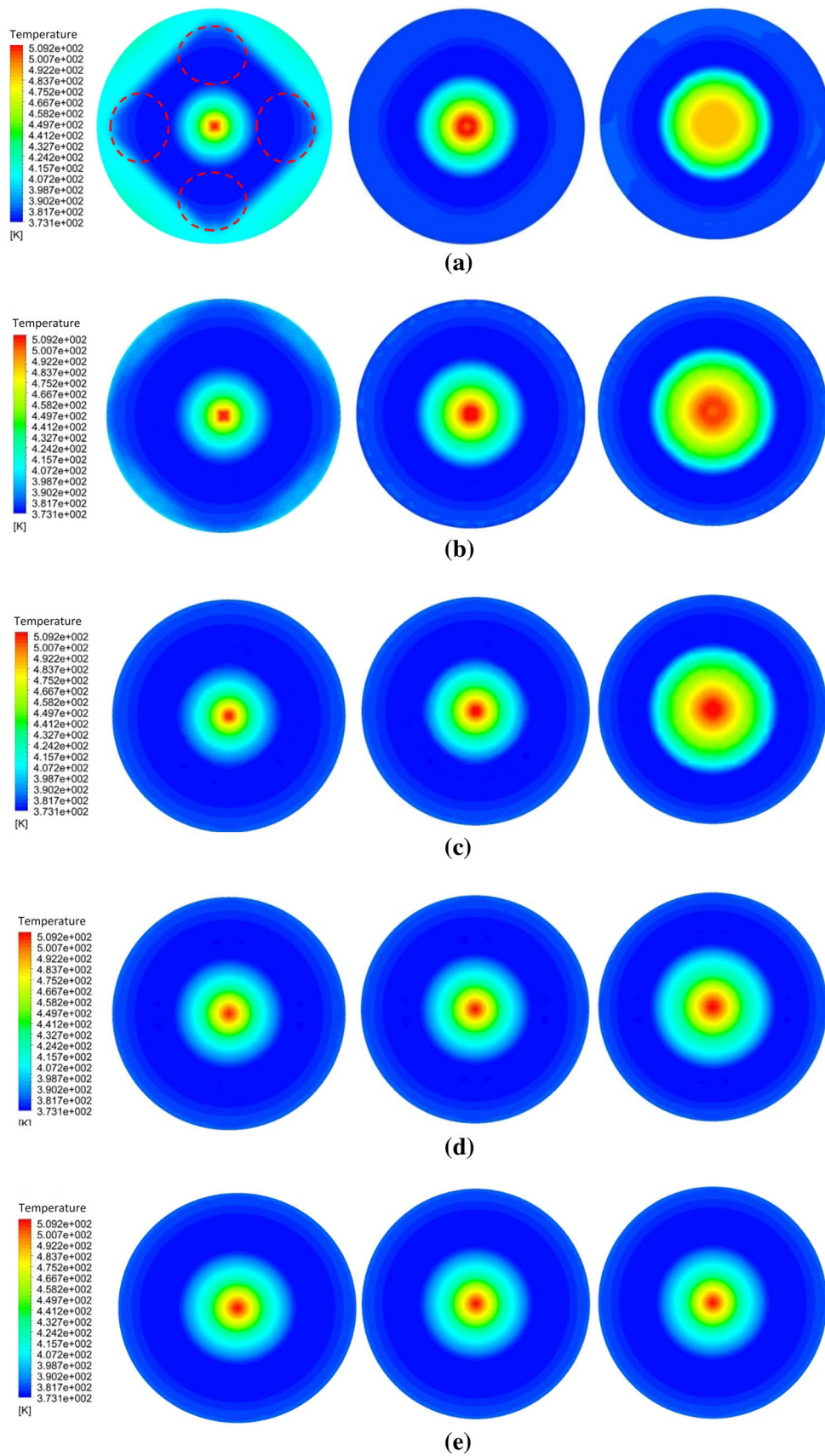


Fig. 7—Gas temperatures for Cases 1–3 (columns 1–3) on five vertical levels (cf. Fig. 4c). (a)  $z = +0.25$  m. (b)  $z = 0.00$  m. (c)  $z = -0.50$  m. (d)  $z = -1.00$  m. (e) Lower domain boundary. Red dashed circles denote locations of gas uptakes (Color figure online).

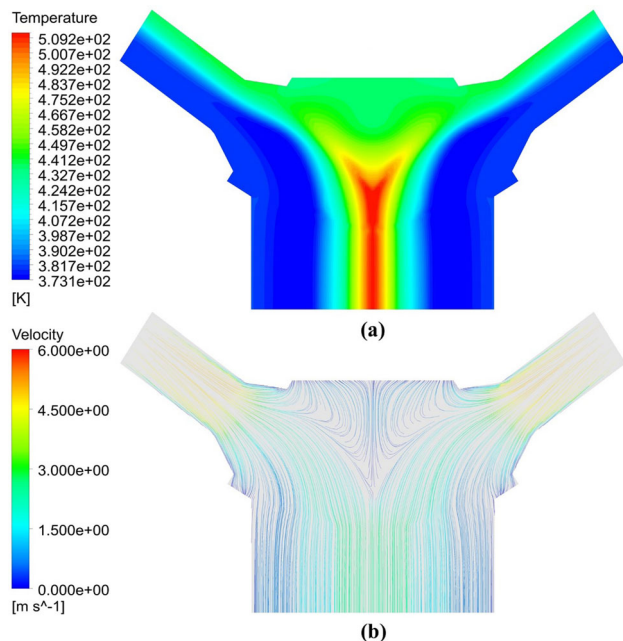


Fig. 8—Center-coke dump (Case 2): (a) Gas temperatures and (b) velocity pathlines for a vertical plane intersecting two gas uptakes (cf. Fig. 4a) (Color figure online).

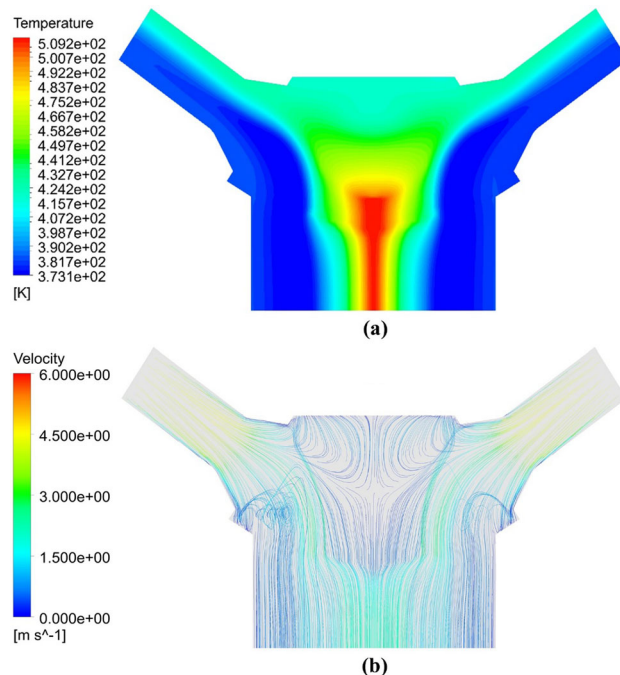


Fig. 10—Center-pellet dump (Case 3): (a) Gas temperatures and (b) velocity pathlines for a vertical plane intersecting two gas uptakes (cf. Fig. 4a) (Color figure online).

above the burden characterized by very low gas velocities. These findings explain the gas temperature fields shown in the top right panel of Figure 7.

### B. Three-Dimensional Views

The considerable differences of the gas flow and temperature observed for different two-dimensional cross sections make it motivated to study the conditions three dimensionally. Figure 14 provides a three-dimensional view of the pathlines in the throat, showing a considerable swirling of the gas after in the region above the burden and before the uptakes.

As it is difficult to discern details in a three-dimensional view, Figure 15 presents quasi-three-dimensional illustrations for Cases 1–3 of the flow fields of gas originating from the vertical plane halfway between two gas uptakes. The throat geometry has been outlined by light lines. The figure clearly explains the motion of the gas between the gas uptakes. For Case 1 (Figure 15(a)), with a strong central gas flow extending to the top of the throat region, the gas is deflected downwards along the conical top walls, creating strong and almost horizontal tornado-like swirls toward the closest two gas uptakes. Detailed scrutiny also reveals a small semi-circular swirl that is deflected into the upper part of each uptake.

Corresponding illustrations of the gas from the same plane for Cases 2 and 3 are provided in Figures 15(b) and (c). These clearly illustrate the lesser extent of the downward flow at the conical top wall, and that the back swirl in the opposite direction above the center-charged dump is also divided in two swirling flows to the top of the closest uptakes. The fact that the main gas flow from the bed is split into two swirl pairs serves to

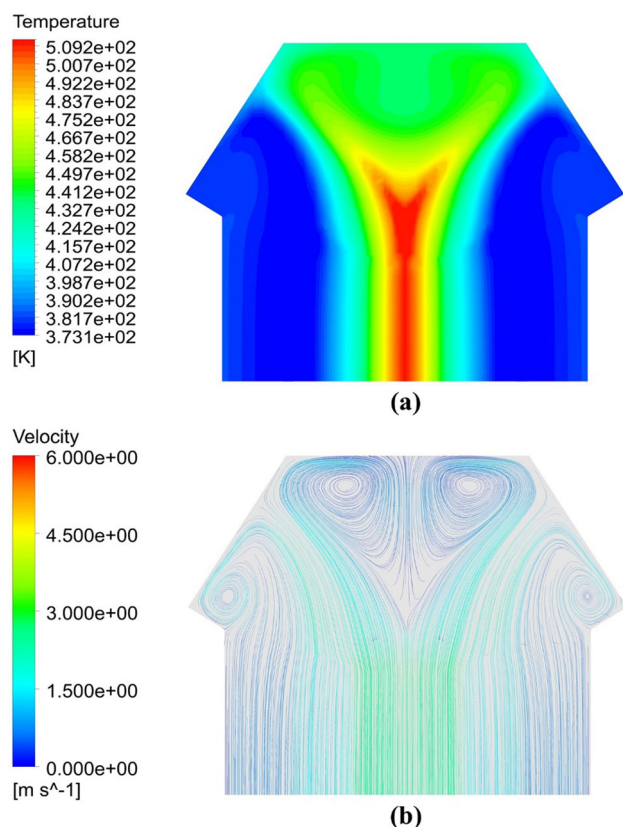


Fig. 9—Center-coke dump (Case 2): (a) Gas temperatures and (b) velocity pathlines for a vertical plane halfway between two gas uptakes (cf. Fig. 4b) (Color figure online).



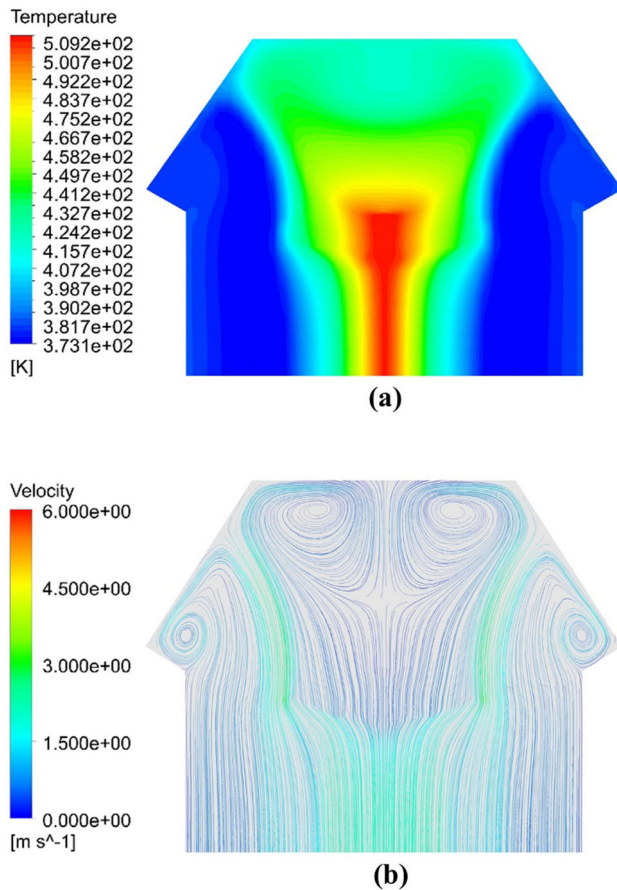


Fig. 11—Center-pellet dump (Case 3): (a) Gas temperatures and (b) velocity pathlines for a vertical plane halfway between two gas uptakes (cf. Fig. 4b) (Color figure online).

decrease the temperature increase observed above the burden surface between the gas uptakes (cf. top middle and right subpanels of Figure 7). It is also interesting to note that the lower swirl for Case 2 (Figure 15(b)) is only directed anti-clockwise. However, this is due to the fact that the plane where the gas originates is taken exactly halfway between the uptakes, so random effects may dictate where the flow (primarily) goes. This can be confirmed by Figure 16, which shows the corresponding flows from a plane rotated 5 deg clockwise from the one depicted in Figure 15(b): now the main flow of the lower swirl goes in the opposite direction.

On the basis of these findings, it is easy to understand that the complex gas flow field above the burden surface has a strong effect on the gas temperature measured by probes or reconstructed by tomographic means based on acoustics. This is particularly true when the distance of the measurement point to the burden surface grows. A further complication is that the gas flow distribution is repeatedly upset by the burden charging, which makes the system strongly dynamic. In the lack of rapid measurements, the observed gas temperatures would therefore represent averages of several different states, which further complicates the interpretation.

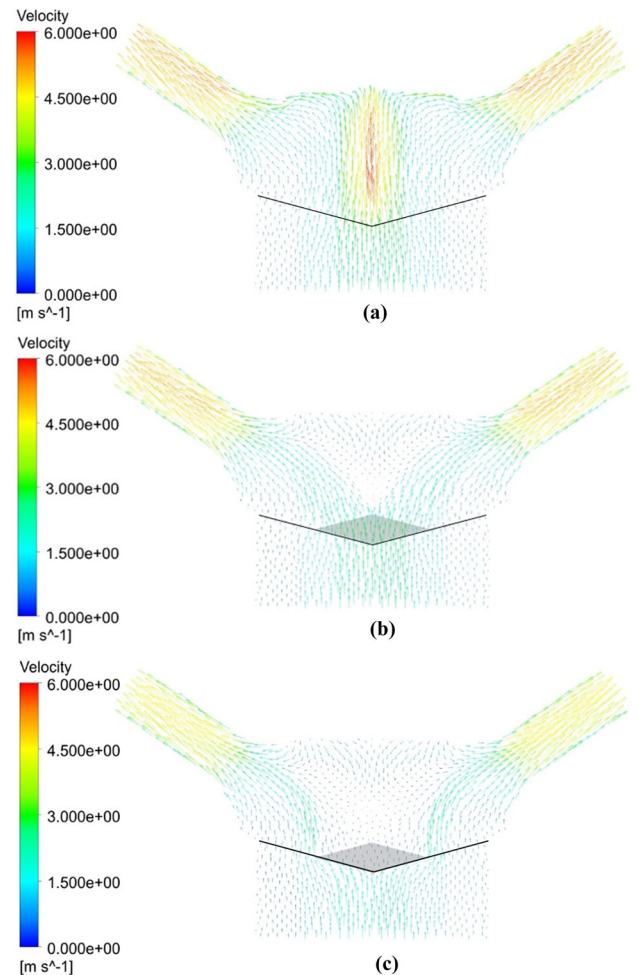


Fig. 12—Gas velocity field for a vertical plane in the throat intersecting two gas uptakes (a) Base bed (Case 1), (b) Base bed and center-coke dump (Case 2), and (c) Base bed and center-pellet dump (Case 3) (Color figure online).

#### IV. DYNAMIC ANALYSIS

The results presented in Section III represent views of the static conditions. However, due to the intermittent charging, the state of the upper part of the blast furnace is never static but is continuously changing. In order to gain an understanding of the dynamics, the redistribution of the gas flow after charging a dump of burden was studied. Starting from the base bed (Case 1), for which the steady-state solution was determined, a center-pellet layer was computationally created. This was undertaken by decreasing the porosity of the cells within the center heap linearly in time from 1 to 0.3 within 5 s (*i.e.*, for  $t = 0$  to  $5$  s). Figure 17 shows a series of snapshots of the dynamics for the vertical plane through two gas uptakes (left panel column) and halfway between the uptakes (right panel column). The top row represents the starting point (*i.e.*, the steady state for Case 1 presented in Figures 5 and 6), while the following panel rows present the states after initiation of the heap ( $t = 0.5$  s), just after the heap has been formed ( $t = 5.5$  s), five seconds later ( $t = 10.5$  s), and finally 15 seconds since the full formation of the heap ( $t = 20$  s), when the new steady state (of Case 3) has been reached. It is seen that

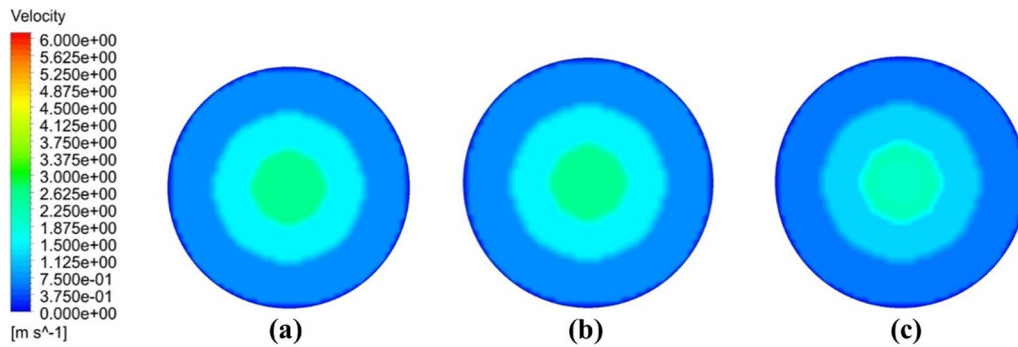


Fig. 13—Gas velocity distribution at the lower end of the simulated domain for (a) Case 1, (b) Case 2, and (c) Case 3 (Color figure online).

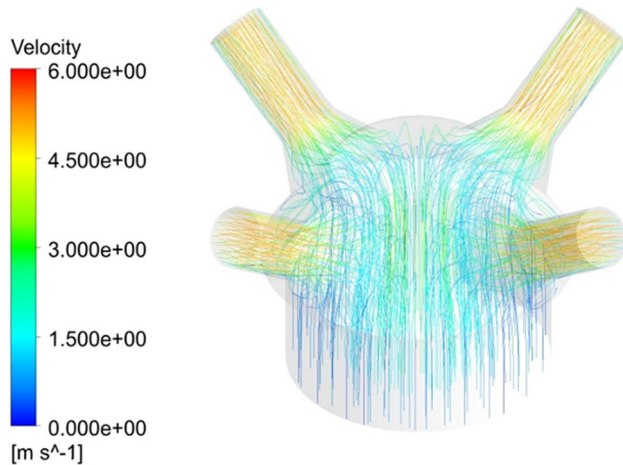


Fig. 14—Three-dimensional view of the pathlines of the gas for Case 1 (Color figure online).

upward gas flow through the pellet heap is gradually replaced by a backflow that grows stronger, while the main flow is diverted to the gas uptakes and the lower swirl between the gas uptakes is suppressed. It is also interesting to note that the backward swirl above the pellet heap is strongest just after the moment when the heap has been fully formed ( $t = 5.5$  s), while the final state shows less intensive backflow. It should be kept in mind that the present model neglects heat transfer from the gas to the burden, which also affects the gas temperature in the throat.<sup>[12,20–22]</sup>

The results indicate that the changes are relatively fast, but still considerably slower than what the average residence time would indicate. The volume between the bed surface and the end of the gas uptakes in the simulated domain is approximately  $80 \text{ m}^3$ , which gives an average residence time of about 3 seconds. For a better visualization, a video of the simulated dynamics is provided in three parts in Ref. 23.

## V. COMPARISON WITH MEASUREMENTS

To compare the results of the computational analysis with findings in the real process, some results from acoustic measurements of the gas temperature in the throats of two operating blast furnaces are presented in

this section. Figure 18 schematically depicts vertical cross sections of the top parts of BF B and BF C, indicating the levels of the burden surface (thick dashed red lines) and gas temperature measuring (thin red dotted line). The furnaces are larger and have a somewhat different design of the top and compared to that of BF A studied in the numerical analysis, which may affect some of the results. In BF B, the acoustic measurement device includes 10 sound generator/microphone pairs located symmetrically on the periphery, while in BF C, a more asymmetric arrangement of the 12 pairs is applied: this is seen in Figure 19, which also illustrates the measuring paths and the reconstructed temperature fields. Figure 20 shows gas temperature estimated based on the acoustic signals at BF B and BF C, representing typical patterns encountered in the operation. While the temperature pattern in BF B is quite concentric, just as observed for the numerical model with suppressed center-gas flow, the results in BF C show clear hot spots (encircled in red) in the region between the gas uptakes (which are indicated by dashed white circles). The latter observations are in general agreement with the simulation results of the base bed (cf. the top leftmost panel of Figure 7). It is obvious that the reason for the hot spots between the gas uptakes seen for BF C is the result of downward-swirling gas (cf. Figures 6 and 15(a)). An explanation for why BF B does not show such local hot spots may lie in the different design of the top of the furnace. In BF B, by contrast to BF A and BF C, the diameter above the cylindrical throat does not expand. The expansion creates favorable conditions for the formation of swirls, while the practically cylindrical geometry in BF B suppresses strong swirls or disperses the downward-flowing gas. Another notable difference between the designs of the tops parts of the three BFs is that the “hat” of BF B is higher and the gas uptake entrances are sitting lower.

Another verification of the redistributing role of the charged burden on the gas flow in the throat was found by a systematic analysis of the temperature patterns in BF B measured after certain dumps. This furnace applies a charging program, where each dump consists of rings built using eleven possible chute angles. Our study focuses on the gas temperatures after charging coke dumps, because these redistribute rather than cool off of the gas because of slower heat transfer to and lower

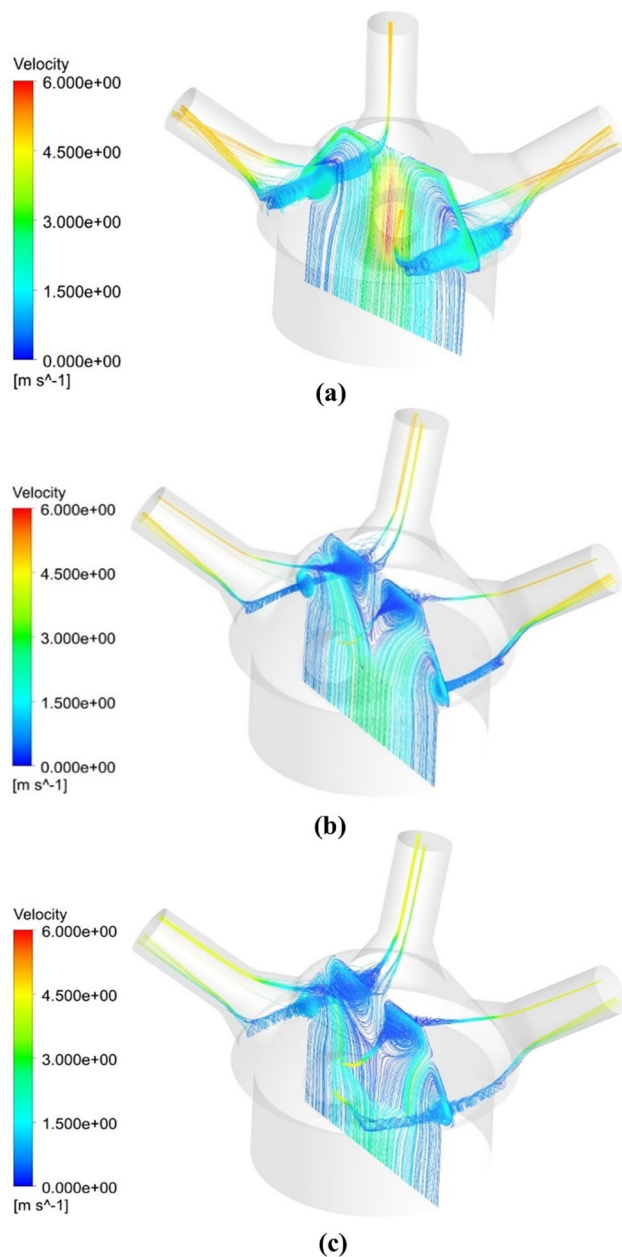


Fig. 15—Quasi-three-dimensional view of the pathlines for gas from a plane exactly halfway between the gas uptakes, with velocities expressed in colors for (a) Base bed (Case 1), (b) Base bed and center coke (Case 2), and (c) Base bed and center pellet (Case 3) (Color figure online).

density of the coke.<sup>[22]</sup> It should be pointed out that the number and therefore also the mass of the coke rings in different dumps can vary, so a dump with fewer rings does not imply that less coke is charged. Further, it should be noted that the charging matrix holds several ore and coke dumps that can be charged differently over the radius. The main intent of our analysis is to investigate how the top gas temperature distribution above the burden surface changes after charging coke dumps that are different in this very respect.

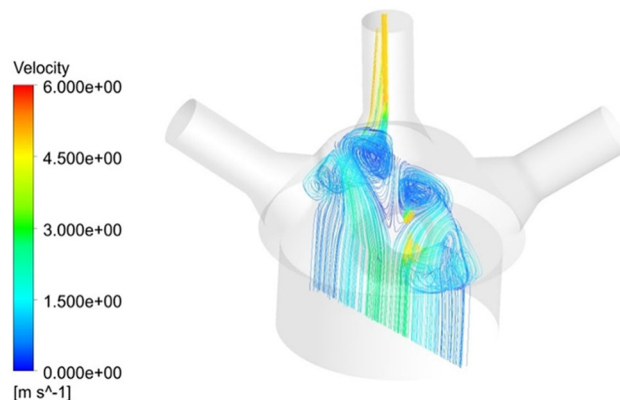


Fig. 16—Quasi-three-dimensional view of the pathlines for Case 2 for gas from a plane 5 deg clockwise from the one depicted in Fig. 15b (Color figure online).

The acoustic gas temperatures between the end of a coke dump and the start of the next (ore) dump were studied for a time period during which different distributions of the coke dumps were applied. At least 1000 temperature patterns for each type of coke dump were extracted, and averages were taken to yield the typical gas temperature patterns corresponding to the coke distribution in question. Figure 21 shows a comparison of six such temperature patterns with the corresponding charging matrix of the coke presented above each subfigure. The digits represent the number of coke rings of the 11 chute positions, starting from the furnace center and ending at the furnace wall. To facilitate a comparison between the patterns, pairs were created which differ with respect to certain parts of the charging matrix, with main focus on the rings charged close to the center, as indicated by arrows. The two types of coke dumps pairs studied in Figures 21(a) and (b) occurred in the same charging matrix but at different positions, so they correspond to exactly the same overall state of the blast furnace. The pairs depicted in Figure 21(c) occurred mostly in different parts of the time period studied, but since the total period length was about two months, the furnace state did not differ fundamentally between these parts. Therefore, it can be concluded that the observed changes in the temperature patterns must primarily be the result of gas redistribution after the coke dumps, and not because of changes in the inner state of the process.

The charging of the two coke layers in the first pair (Figure 21(a)) differs only with respect to the number of coke rings at the second chute position, where this number is decreased from 4 to 2. The result is a decrease in the extent of the high-temperature zone (green and yellow in the figure) because of less blocking of the furnace center. In the second pair (Figure 21(b)), where no coke is charged in the first and second positions (which result in clearly stronger central gas flow), a decrease of the number of rings in the third position from 4 to 1 enhances the central gas flow and increases the size and temperature of the “hot eye” (yellow) in the



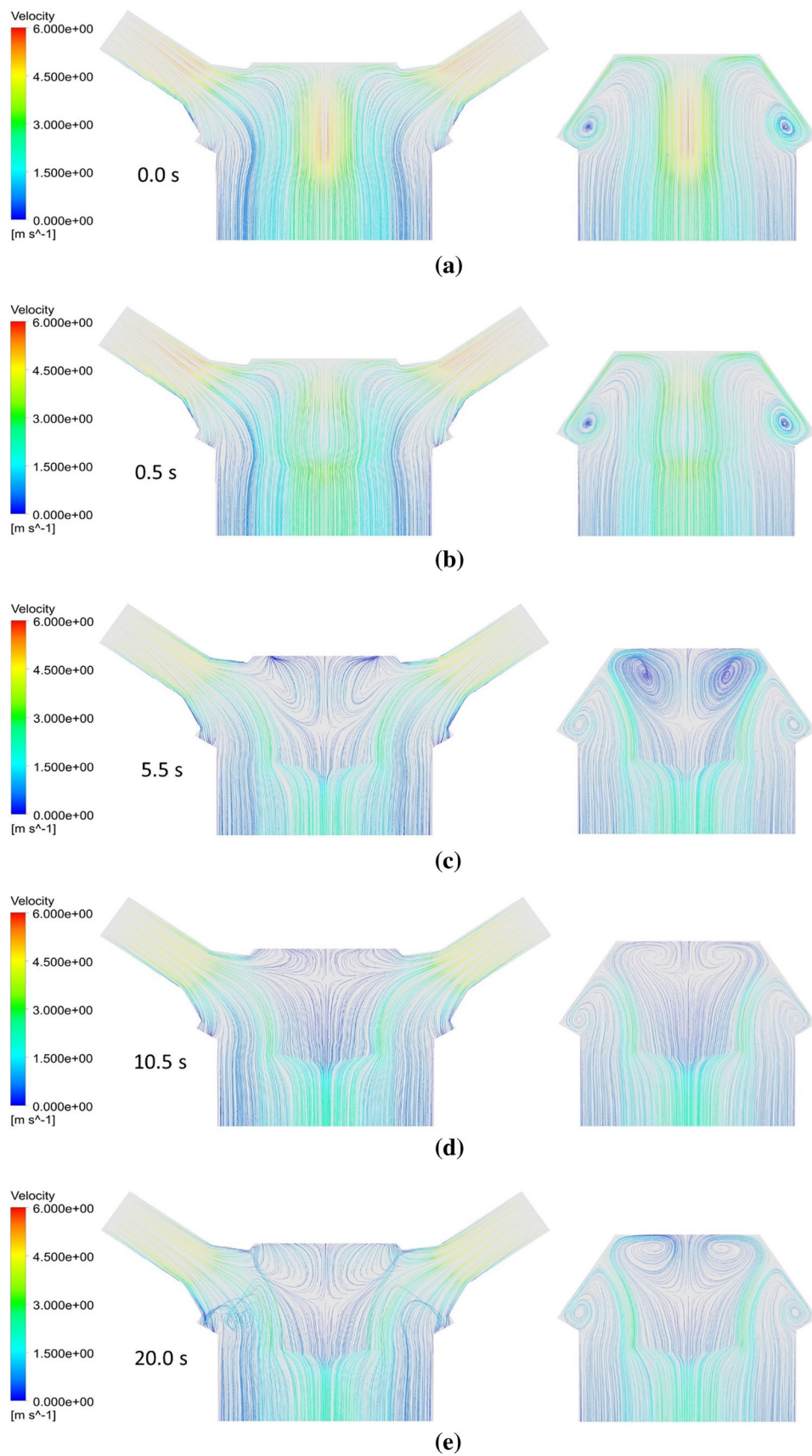


Fig. 17—Dynamics of the flow from Case 1 to Case 3 for cross sections through (left column) or between (right column) the gas uptakes. (a) A center-pellet heap is created for  $t = 0 \dots 5$  s, (b) The state 0.5 s after initiation of the heap, (c) The state 0.5 s after complete formation of the heap, (d) The state 5 s after the heap is formed and (e) The new steady state reached 15 s after the heap has been formed (Color figure online).



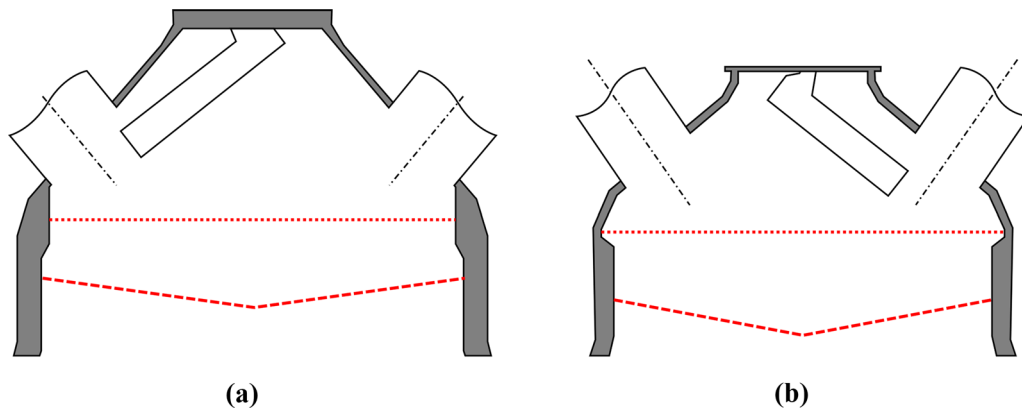


Fig. 18—Schematics of the top (a) BF B and (b) BF C equipped with acoustic gas temperature measurements on the levels indicated by horizontal dotted lines. Dashed lines show the approximate burden surface levels in the furnaces.

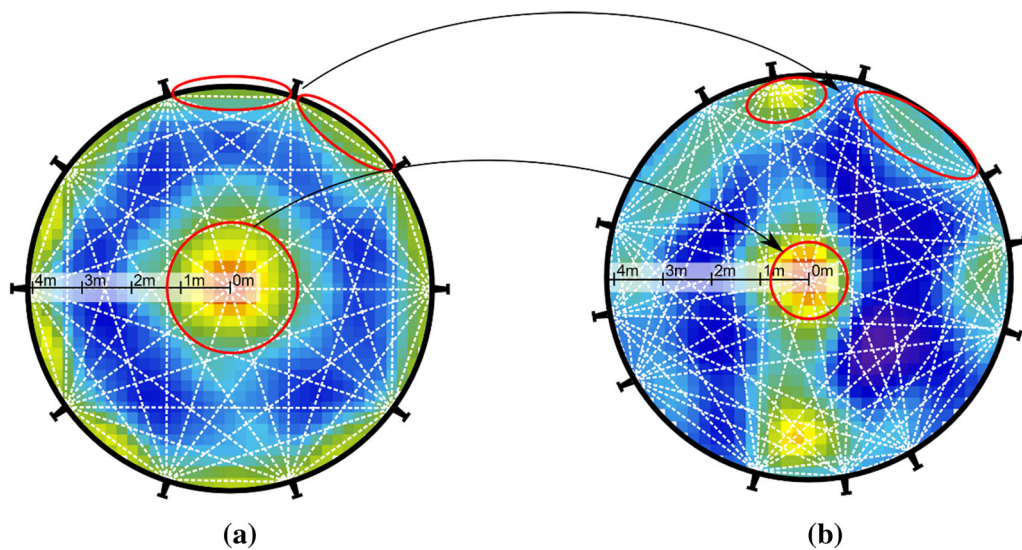


Fig. 19—Locations of the acoustic source and microphones, measuring paths between these. Examples of reconstructed temperature fields for (a) BF B and (b) BF C are also depicted (Color figure online).

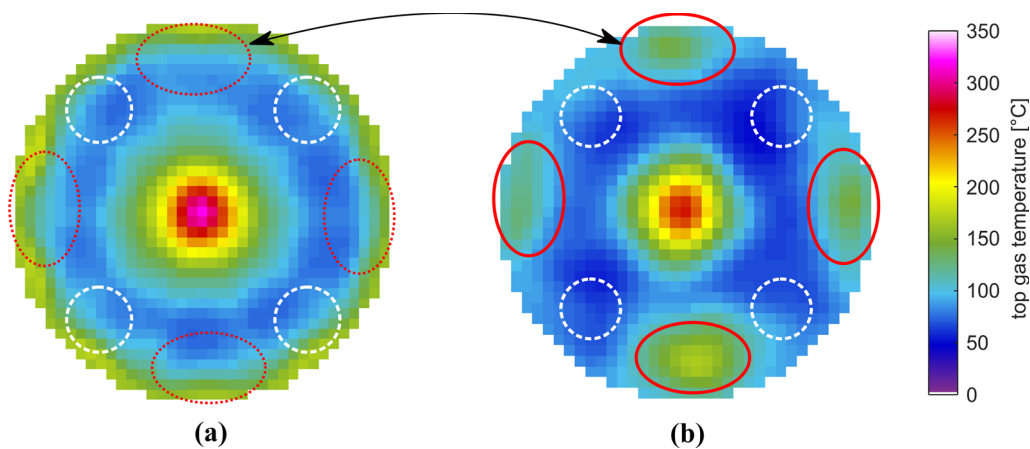


Fig. 20—Typical temperature distributions estimated by the acoustic measurement in (a) BF B and (b) BF C. The locations of the four gas uptakes are indicated by white dashed circles, while the regions between these are encircled by red ovals (Color figure online).

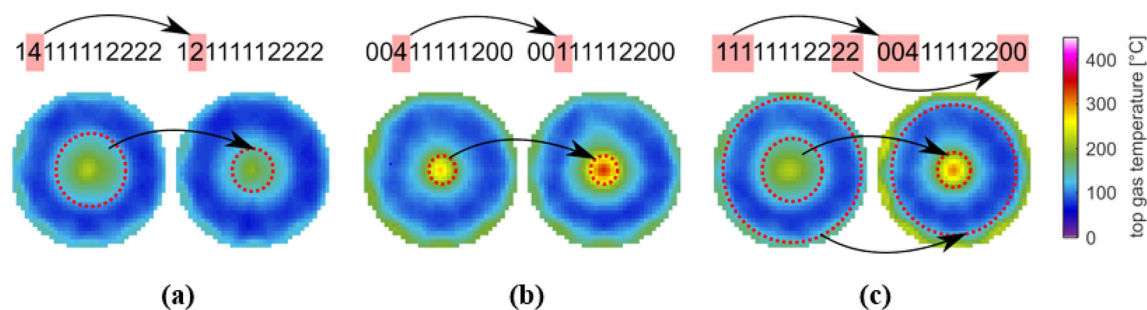


Fig. 21—Average gas temperature distribution after charging layers of coke inducing temporal redistribution of the gas flow. The digit series above each pattern represents the number of coke rings for every chute position from the furnace center to the wall. (a) Decrease of coke rings charged with chute position 2, (b) decrease of coke rings charged with chute position 3, and (c) decrease of coke rings charged with chute positions 1–2 and 10–11 (Color figure online).

center. Finally, the third pair (Figure 21(c)) shows the effect of shifting rings from both the center and the wall to intermediate positions. The outcome is stronger central and wall flows with higher temperatures, while suppressed flow and temperatures occur at the intermediate points. These observations support the findings in the numerical analysis concerning the gas redistribution caused by the charged dumps.

## VI. CONCLUSIONS AND FUTURE WORK

This work has studied the gas temperature and flow distribution in the throat of the blast furnace by using a CFD model, which considers the mixing of the gas but neglects heat transfer to the bed and walls. Simulations have revealed that strong redistribution and downward-swirling flows may occur, which affect measurements of the gas temperature above the burden surface. Different states of the upper part of the burden have been studied and it has been demonstrated that the charging of dumps in the center part strongly modifies the flow patterns, and therefore also the measured temperatures in the throat. A brief study of the dynamics of the system has also been undertaken, indicating that the gas flow pattern stabilizes within 20 seconds after a dump. Acoustic gas temperature measurements in two industrial blast furnaces have shown similar patterns, verifying the downward swirl of gas between the gas uptakes, which elevates the temperatures locally. The findings of the computational study have provided information about the gas flow patterns that can be used for better interpretations of temperatures from probes or from tomographic techniques. The model could, for instance, be used to study the optimal location of measurements. The results are also expected to be useful for studies of the feasibility of future acoustic temperature measurements that are faster than the present state-of-the-art technology and how such information could be used to shed more light on the conditions in the upper part of operating blast furnaces. Topics left for future studies are to validate the model by comparison with extensive sets of measured temperatures and possibly to consider the heat transfer between the gas and the burden.

## ACKNOWLEDGMENTS

The research was initiated with funding from the European Union's Research Fund for Coal and Steel (RFCS) research program under Grant Agreement No. 709816 (StackMonitor) and finalized under the Platform Economy in Metals Processing (AMET) project. The financial support of the European Commission, Business Finland and participating companies is gratefully acknowledged.

## FUNDING

Open access funding provided by Abo Akademi University (ABO).

## CONFLICT OF INTEREST

On behalf of all authors, the corresponding author states that there is no conflict of interest.

## OPEN ACCESS

This article is licensed under a Creative Commons Attribution 4.0 International License, which permits use, sharing, adaptation, distribution and reproduction in any medium or format, as long as you give appropriate credit to the original author(s) and the source, provide a link to the Creative Commons licence, and indicate if changes were made. The images or other third party material in this article are included in the article's Creative Commons licence, unless indicated otherwise in a credit line to the material. If material is not included in the article's Creative Commons licence and your intended use is not permitted by statutory regulation or exceeds the permitted use, you will need to obtain permission directly from the copyright holder. To view a copy of this licence, visit <http://creativecommons.org/licenses/by/4.0/>.

## REFERENCES

1. S. Kuang, Z. Li, and A. Yu: *Steel Res. Int.*, 2018, vol. 89, p. 1700071.

2. P. Abhale, N.N. Viswanathan, and H. Saxén: *Min. Proces. Extr. Met.*, 2020, vol. 129, pp. 166–83.
3. Y. Omori (Ed.), *Blast Furnace Phenomena and Modelling*, The Iron and Steel Institute of Japan, Elsevier, London, 1987.
4. M. Geerdes, H. Toxopeus, and C. van der Vliet: *Modern Blast Furnace Ironmaking: An Introduction*, 2nd ed. IOS Press BV, Amsterdam, 2009.
5. S. Seetharaman: *Treatise on Process Metallurgy, Volume 3: Industrial Processes, Part A*, American Elsevier Company, New York 2014.
6. I. Cameron, M. Sukhram, K. Lefebvre, and W. Davenport: *Blast Furnace Ironmaking: Analysis, Control, and Optimization*, 1st ed. Elsevier, Amsterdam, 2020.
7. K. Narita, S. Inaba, M. Shimizu, A. Yamaguchi, I. Kobayashi, and K. Okimoto: *Trans. ISIJ*, 1981, vol. 21, pp. 405–13.
8. J. Jiménez, J. Mochón, and J.S. De Ayala: *ISIJ Int.*, 2004, vol. 44, pp. 518–26.
9. J. Park, U. Baek, K. Jang, H. Oh, and J. Han: *ISIJ Int.*, 2011, vol. 51, pp. 1617–23.
10. Z.Y. Li, S.B. Kuang, S.D. Liu, J.Q. Gan, A.B. Yu, Y.T. Li, and X.M. Mao: *Powder Technol.*, 2019, vol. 353, pp. 385–97.
11. T. Iwamura, H. Sakimura, Y. Maki, T. Kawai, and Y. Asano: *Trans. ISIJ*, 1982, vol. 22, pp. 764–73.
12. H. Saxén, M. Nikus, and J. Hinnelä: *Steel Res.*, 1998, vol. 69, pp. 406–12.
13. R. Timmer: *Quantitative description of the gas flow pattern in the blast furnace throat area*, Technical Steel Research, European Commission, Report EUR 16778, 1997.
14. R. Timmer, J. Droog, G. Flierman, and A. Steeghs: *Steel Res.*, 1997, vol. 68, pp. 47–53.
15. M. Tonteling, H. Rausch, A. Oliveira, C. Bodeving, and D. B. M. Cruz: *Seminário de Redução de Minério de Ferro e Matérias-Primas e o 14º Simpósio Brasileiro de Minério de Ferro*, 2013, vol. 43, pp. 345–55.
16. J. F. Stumper, M. Krüssmann, C. Bodeving, and D. B. M. Cruz: *44th Ironmaking and Raw Materials Seminar*, 2014, Belo Horizonte, pp. 1162–75.
17. G. Behler and J.G. Richter: *J. Acoust. Soc. Am.*, 2016, vol. 140, p. 3375.
18. R. Lin, H. Rausch, W. Hartig, and L. Wu: *BHM Berg- Huettenmaenn. Monatsh.*, 2017, vol. 162, pp. 41–49.
19. L. Shi, Y. Wen, G. Zhao, and T. Yu: *J. Iron Steel Res. Int.*, 2016, vol. 23, pp. 203–09.
20. M. Nikus and H. Saxén: *ISIJ Int.*, 1996, vol. 36, pp. 1142–50.
21. H. Saxén and M. Nikus: *ISIJ Int.*, 2002, vol. 42, pp. 115–17.
22. D.N. Mondal, H. Wei, Y.W. Yu, and H. Saxén: *Steel Res Int.*, 2022, vol. 93, p. 220035.
23. Available from: <https://youtu.be/a3biNydKrCg>, <https://youtu.be/10xr3dicCjM>, <https://youtu.be/xxopmCE-rC0>.

**Publisher's Note** Springer Nature remains neutral with regard to jurisdictional claims in published maps and institutional affiliations.